A Mechanistic Study of the Methanol Dehydration Reaction on γ-Alumina Catalyst

Rinaldo S. Schiffino*,† and Robert P. Merrill

School of Chemical Engineering, Cornell University, Ithaca, New York 14853

Received: January 4, 1993; In Final Form: March 31, 1993

The dehydration of methanol over a porous γ-Al_2O_3 catalyst was studied using periodic square-wave modulation of the feed to a microcatalytic reactor. Online mass spectrometry was used to obtain wave forms at the exit of the reactor for methanol, dimethyl ether, water, and a carrier gas. The reaction was studied over the temperature range of 230–350 °C. At lower temperatures, the dimethyl ether wave form went first through a maximum, decreased to a constant level during the on cycle, and then went through a second maximum at the beginning of the off cycle. At higher temperatures where the conversions increased, the relative intensity of the maximum to the level part of the wave form continuously decreased until no maximum could be observed at temperatures above 280 °C. Water was found to have a phase lag of about 4 s with respect to dimethyl ether over the studied temperature range. The shape of the wave forms was explained in terms of a reaction mechanism which involved reactions of surface species formed from the adsorption of methanol on the γ-Al_2O_3 surface. The species considered were molecularly adsorbed methanol, methoxy, and hydroxyl groups. The mechanism contained two parallel reaction pathways for the production of dimethyl ether. One pathway was the reaction between molecularly adsorbed methanol and methoxy species, and the other was the reaction between two methoxy species. For the production of water, only a single step of recombination of surface hydroxyls was considered in the mechanism. Equations for the material balances of the species considered in the mechanism were numerically integrated to generate wave forms with the same shape as observed in the experimental data.

Introduction

Porous catalysts have been widely used in industrial chemical processes. There are many examples of catalytic reactions where a porous material is impregnated with the solid catalyst and placed in a chemical reactor to contact a fluid mixture containing reactants. The reactants adsorb on the catalyst surface and undergo a sequence of elementary reactions on the surface to form the products. The products desorb back to the fluid phase. The chemical formulation of the solid catalyst, the method of impregnation of the porous matrix, and the pretreatment of the catalyst before the reaction affect the sequence of surface reactions leading to different selectivity and productivity of the chemical reactor. There is considerable interest in understanding the mechanism by which the catalyst acts in order to design improved catalysts or to find more profitable operating conditions for known catalysts.

The sequence of elementary reactions which take place on the surface of such catalysts can be formulated at several levels of complexity and molecular detail. For example, upon adsorption, the reactant molecules may dissociate by breaking a chemical bond into two different surface species and the products may be formed from subsequent reactions of these species. In the case of the porous catalyst of industrial practice, reaction sequences can usually be formulated to the extent that there is evidence for identifiable surface intermediates. Reaction sequences are often proposed from a set of experimental data on a particular reaction and catalyst system by fitting the results of the proposed model to the empirical behavior of the system.

Dynamic experiments serve well for the study of reaction sequences. By disturbing the feed concentration to a chemical reactor and measuring the product response, information about possible reaction sequences is obtained. The output response forms a residence time distribution and may under carefully controlled conditions reflect the residence time of the species on the surface. The surface residence time distributions contain inductive information about the reaction sequence and are independent of the input function.

In addition to reaction mechanism studies, the dynamic or periodic operation of chemical reactors has been proposed as a way to increase selectivity and yield of chemical reactors. Several theoretical studies for different kinetic schemes have been published in the late 1960s and early 1970s by Douglas,[1] Horn and Lin,[2] Bailey and Horn,[3] Bailey,[4] and Renken.[5] Renken[6] reviewed the concepts for the selection of reaction schemes that could present improved performance under unsteady-state conditions, as opposed to the conventional steady-state operation. In general, systems in which the governing mass balances contain nonlinear terms, either from nonlinear kinetics or from the exponential temperature dependence of the rate constants, are good candidates to have improved performance under periodic operation. The benefits in selectivity were more pronounced in complex reacting systems where parallel reaction pathways lead to different yields.

More recently, Silveston[7] reviewed the experimental literature on periodic operation of chemical reactors covering applications where catalyst activity was improved. Examples were given of periodic operation in several chemical systems, such as ammonia synthesis, sulfur dioxide oxidation, automotive catalysts, carbon monoxide oxidation, methanol synthesis, and Ziegler–Natta polymerizations. In the study of oxidation of SO_2 over a V_2O_5 catalyst, Unni et al.[8] found that significant increases in the rate of oxidation could be obtained by the periodic modulation of the SO_2/O_2 ratio in the feed to the catalyst bed. It was concluded that the periodic operation improved the performance in terms of capacity increases, but it would not alter the overall conversion because the SO_2 oxidation was an equilibrium-limited reaction over the studied temperature range.

Renken et al.[9] found that the yield and selectivity of the ethylene oxidation over a silver catalyst could be remarkably increased by the periodic operation. A decrease in the hot spot temperature and an increase in the ignition temperature allowed the reaction to be carried out closer to the optimum temperature, resulting in better selectivity. The results were qualitatively explained by the higher loading of the catalyst surface with molecular O_2 favoring the oxidiation of ethylene to ethylene oxide as opposed to total oxidation reaction which took place on sites with adsorbed

† Present at Exxon Chemical Co., Baytown, TX 77520.

0022-3654/93/2097-6425$04.00/0

atomic oxygen. Bilimoria and Bailey[10] found that the selectivity of the hydrogenation of acetylene to ethylene on nickel catalyst could be improved by fluctuating the H_2 flow. Under isothermal periodic operation, an overshoot in the ethylene production was observed when the H_2 flow was switched to the high-level value. This overshoot was a result of the presence of nonlinear dynamics in the system.

Dettmer and Renken[11] found that the vinyl acetate production from acetic acid and ethylene on SiO_2 catalyst was dramatically increased over the steady-state value when the acetic acid concentration was periodically varied under a constant ethylene concentration. This improvement of the vinyl acetate production was explained by a buildup of the ethylene concentration on the catalyst surface during the off cycle of the acetic acid concentration wave. This finding was explored in a related patent (U.S. 4,-128,727, 1978), where the authors proposed a process for the production of vinyl acetate in a fixed bed reactor operated under variable acetic acid concentration with cycles of approximately 10 min.

In summary, the review of examples of periodic operation of chemical reactors showed that the improvement over the steady-state case depended on the period of the perturbations, the duty cycle, the average reactant composition, and, more importantly, the type of reaction mechanism present. In a mechanistic study, Siddall et al.[12] conducted pulsed experiments on the methane synthesis reaction from carbon monoxide and hydrogen using a cobalt and a supported-ruthenium catalysts. They found that the coverage of reaction intermediates increased with temperature and with the H_2/CO ratio. The study also suggested that the rate-limiting step of CO dissociation could be increased by the presence of hydrogen. The pulsed experiments were conducted with a computer-operated mass spectrometer to measure concentrations on a time scale comparable to the kinetic effects, e.g., of the order of seconds. Argon was used as a carrier gas to facilitate the separation of hydrodynamic effects from the laboratory reactor data. These experimental techniques were similar to those used in the research to be described here.

In this research, the reaction of the dehydration of methanol to produce dimethyl ether and water was studied under periodic operation:

$$2CH_3OH(g) \leftrightarrow CH_3OCH_3(g) + H_2O(g)$$

Industrially, this reaction is important when methanol is considered as an alternative raw material for petrochemicals. The subsequent dehydration of dimethyl ether leads to ethylene, an essential starting chemical for several petrochemical processes. With the understanding of the reaction mechanism, new processes and catalysts can be designed that give methanol a competitive position with traditional fossil fuels as an ethylene raw material. In this study, the objective was to obtain mechanistic information about the methanol dehydration reaction from data obtained in a laboratory reactor operated under periodic operation.

The methanol dehydration reaction is a reversible reaction with a low heat of reaction (–5.63 kcal/mol at 25 °C) and high conversions at equilibrium in the temperature range of 200–350 °C. The equilibrium constant for the reaction was calculated as a function of the temperature using ideal gas heat capacities. Truncating the expression of the equilibrium constant to the first two leading terms in temperature, the following expression was obtained (T in K):

$$\ln K(T) = -1.7 + \frac{3220}{T} \quad (1)$$

The methanol conversion at equilibrium was obtained as a function of the temperature by the following expression:

$$\% X_{eq} = \frac{4K(T) - 2K(T)^{0.5}}{4K(T) - 1} \quad (2)$$

The solid line in Figure 1 shows the plot of the methanol conversion at equilibrium as a function of temperature. The conversions are between 90% and 100% for the temperature range of 150–400 °C, and they decrease with increasing temperature because of the exothermic reaction. For comparison, steady-state experimental conversions are also shown in Figure 1. The data show that for temperatures above about 280 °C, the conversions become constant or approximately lower, indicating that the reaction approached thermodynamic equilibrium.

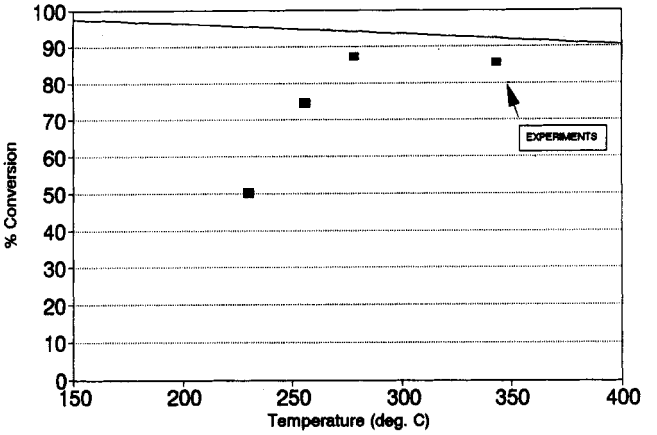

Figure 1. Conversions at equilibrium: MeOH dehydration on alumina.

The methanol dehydration reaction is catalyzed by γ-Al_2O_3, a transition alumina. Aluminas are traditionally prepared by dissolving the mineral bauxita under pressure, under heat, and in caustic soda to form a sodium aluminate solution.[13] After separation of undissolved impurities, gibbsite (α-Al_2O_3 trihydrate) containing 2–3% H_2O is precipitated from the solution.[14,15] Transition aluminas (χ-, η-, κ-, and θ-aluminas) are formed upon heating of gibbsite at various conditions. γ-Al_2O_3 is formed by rapid heating of gibbsite at about 400–500 °C in the presence of moist air and small amounts of alkali metals. The use of large particle sizes reduces the rate of loss of water by diffusion and promotes hydrothermal reactions, resulting in solids of high surface area (typically 250–350 m^2/g). By further heating above 1100 °C, all transition aluminas are converted to the stable, dense, and low surface area α-alumina. All aluminas prepared at about 300 °C are stable and are not hydrated but contain small amounts of water of constitution (γ-Al_2O_3 contains about 0.5%). The thermal stability of γ-Al_2O_3 is improved by adding 1–5% silica, which presumably forms a viscous film of silicate in the grains boundaries and isolates the alumina crystallites. Silica may also increase the acidity of the catalyst.

The ideal surface of ionic γ-Al_2O_3 crystal can be modeled by truncating the bulk structure at a preferentially exposed face. According to Lippens and Steggerda,[16] these faces are the (100) and the (110) planes. For energetic reasons, the crystallites terminate only on anion layers with cation layers underneath. The aluminum cation sites in tetrahedral and octahedral sites. In order to satisfy the Pauling's electrostatic valence rule that the net charge in a stable ionic structure should be equal to or nearly equal to zero, the surface layers should be of OH groups rather than oxygen anions. Furthermore, oxide surfaces are usually covered with hydroxyl groups formed by chemisorption of water.[17]

Experiments have shown that aluminas must be pretreated to about 300–400 °C for the development of catalytic activity.[18] The removal of hydroxyls as water from the alumina surface is essential for catalytic activity. The dehydration of the ideal (100) surface has been modeled by Peri[17] and Dabrowski et al.[19] Applying the Monte Carlo method to a square lattice of the fully hydrated surface, Peri found that the maximum removal of OH groups was 67% if local order was maintained. If defect formation such as vacancies of surface oxides was allowed, the removal was 90.4%. Further removal was only possible with migration of surface ions. For the remaining OH, after the 90.4% removal level, five possible configurations of OH were found which

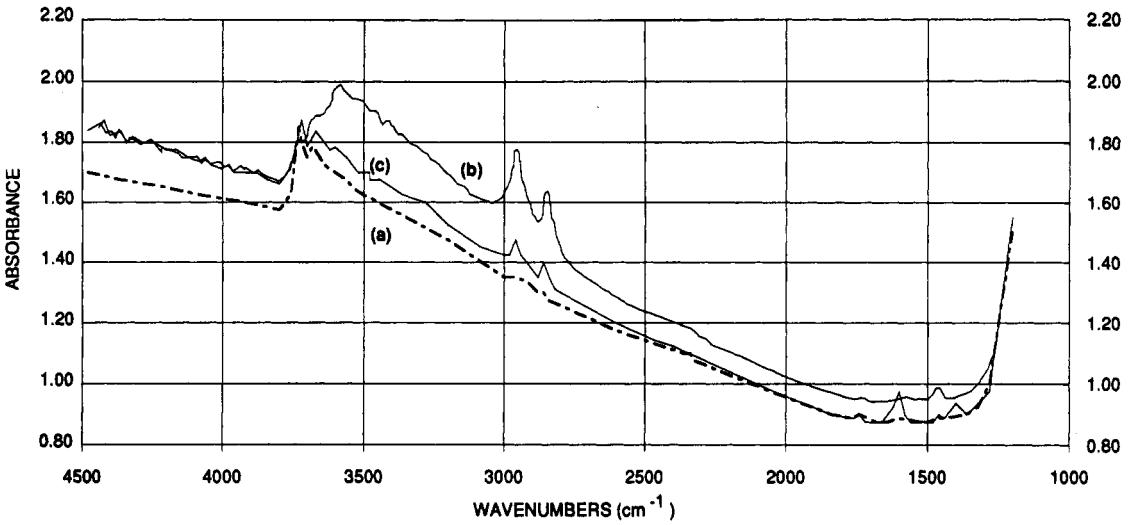

Figure 2. FT-IR spectra of γ-Al_2O_3 in vacuum at 100 °C: (a) heating at 450 °C; (b) exposure to methanol at 300 °C; (c) heating at 450 °C following methanol exposure.

corresponded to different arrangements of OH having up to four nearest oxide neighbors. With removal of OH, aluminum ions of the bottom surface layer became exposed for adsorption of "electron-rich" molecules. Peri's model overestimates the number of catalytically active sites for some reactions, indicating that there might be several types of defects on the surface with different activity levels for different reactions.

The chemisorption of molecules on the γ-Al_2O_3 can be visualized by applying the Lewis acid–base concept to the interaction of the surface with adsorbates.[20] The result of the interaction of an acid, or electron acceptor, with a base, or electron donor, is the formation of an acid–base adduct complex. In the case of surfaces, the acid and basic sites may be localized on a single atom or delocalized over several atoms and the surface can be an acid with respect to one absorbate or a base with respect to another or have both characters simultaneously. In the case of γ-Al_2O_3, the electron-rich oxygen anions show basic character and the electron-deficient aluminum cations show acidic character. The exposure of aluminum cations after the dehydration process allows the attack of these cations by the oxygen electron lone pair of the methanol molecule, resulting in the formation of a molecularly, undissociated, and coordinated methanol. This surface species are referred to as molecularly adsorbed methanol.

Upon heating, the molecularly adsorbed methanol can dissociate to form a methoxy group. The dissociation might takes place when the molecularly adsorbed methanol falls into a bridged position coordinating to more than one aluminum cation.[21] This additional coordination favors the dissociation of the OH group by transfer of the proton to an adjacent basic site with the formation of a surface hydroxyl. Other forms of adsorbed methanol molecules, such as a hydrogen-bonded molecule on the top of the oxide or a complex species with partial coordination to the aluminum and partially hydrogen bonded to an nearby oxide, have been identified in microcalorimetric and spectroscopic studies, but only the molecularly adsorbed methanol has been considered as a precursor for the formation of methoxy groups on the surface.

The presence of methoxy species on the γ-Al_2O_3 can be detected by FT-IR spectroscopy. Figure 2 shows an example of an FT-IR study that detected hydroxyls and methoxy species.[22] These infrared studies were carried out on a sample of the Harshaw 1602 catalyst mounted into a vacuum system of an FT-IR instrument. The sample was pressed into a pellet about 1 cm in diameter and weighing 6.8 mg. All spectra were taken in vacuum at 100 °C following treatment of the sample with respect to temperature or methanol exposure. The spectrum shown by line a was taken after the sample was heated at 450 °C for 10 min, by line b after the sample was exposed to 70 Torr of methanol at 300 °C, and by line c after heating again at 450 °C for ten min following the methanol exposure. Spectrum a shows bands at 3730 and 3675 cm^{-1}, indicating the presence of hydroxyls that remained in the sample after the partial dehydration at 450 °C (residual hydroxyls). Spectrum b shows a broad band from 3800 to 3200 cm^{-1} and a pair of bands at 2950 and 2850 cm^{-1}, which represent modified O–H stretching and C–H stretching modes of methoxy species, respectively. The assignment of the methoxy bands follows the study by Busca et al.[21] of the methanol adsorption on alumina. Spectrum c shows the recovery of the bands at 3730 and 3675 cm^{-1}, the reduction of absorbance of bands at 2950 and 2850 cm^{-1}, and the appearance of bending features from 1800 to 1300 cm^{-1}. This last spectrum indicates that the residual hydroxyls can be recovered after methanol desorption and that part of methanol is not evacuated at 450 °C. No bands from molecularly adsorbed methanol would be seen in these spectra, because this species desorbs at 300 °C under vacuum.

The reaction rate for dimethyl ether formation has been found to follow a Langmuir–Hinshelwood type of expression.[23] The possibility of a reaction of methanol gas with adsorbed species following the Rideal–Eley mechanism has not been considered, because the reaction rate has been determined as zero order on the methanol concentration. Therefore, the dimethyl ether formation has been described by a surface reaction between adsorbed species.[24,25] Some authors have suggested the reaction involves two distinct species: molecularly adsorbed methanol and methoxy groups.[21,23] Others suggested that it involves species of the same type: two methoxy groups. There is no evidence in favor of a reaction mechanism involving two distinct or equal surface species in the dimethyl ether (DME) formation.

In summary, the methanol dehydration reaction on the surface of γ-Al_2O_3 has two intermediates for the production of dimethyl ether and water: the methoxy and the hydroxyl groups. Both species can have long residence times on the surface and are produced from the dissociation reaction of methanol upon adsorption. In this research, interesting kinetic behavior was found in the temperature range of 230–340 °C, which corresponded to strong methanol adsorption in the lower temperature range and to weaker adsorption in the higher temperature range, as shown in the desorption study by Matsushima and White.[26] The following experimental apparatus was assembled to study the transient kinetics of the DME formation from methanol on γ-Al_2O_3 catalyst.

Experimental Apparatus

The experimental apparatus is shown in Figure 3. Helium and argon were carrier gases, and methanol was added to the argon stream in the saturator. The gases were fed through a

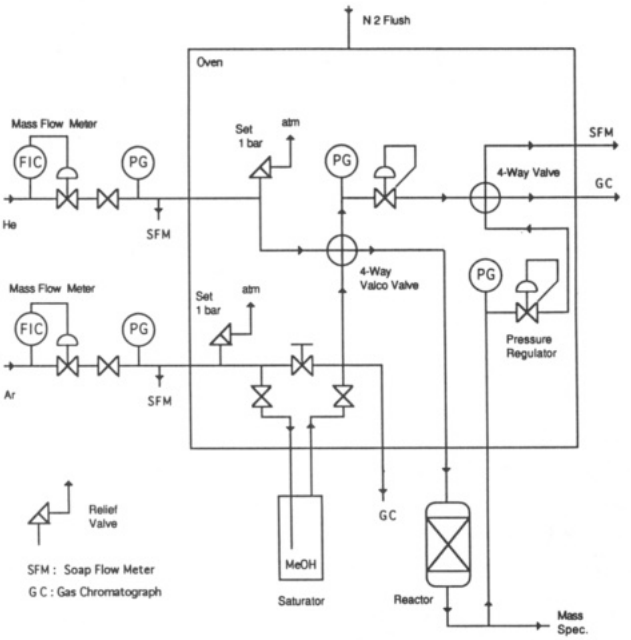

Figure 3. Experimental apparatus.

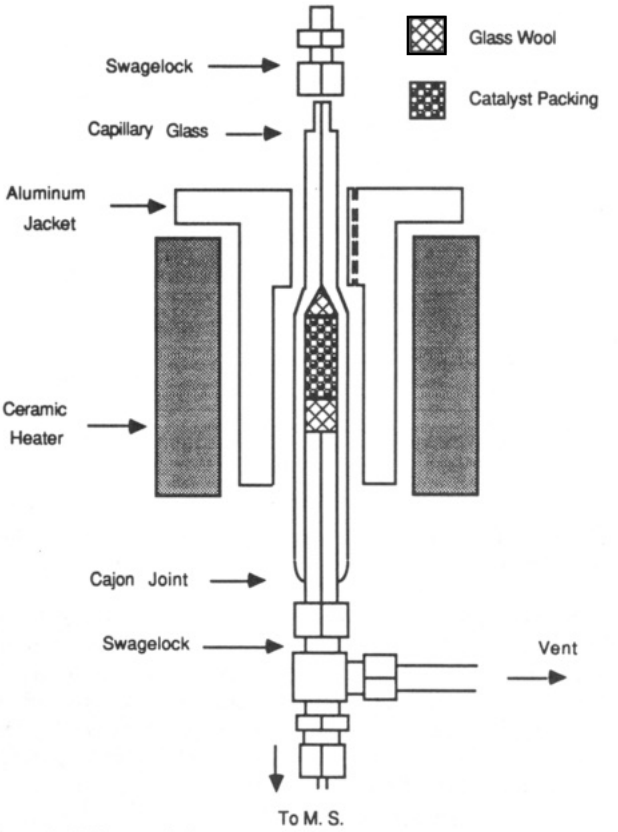

Figure 4. Microcatalytic reactor.

four-way Valco valve (the modulator) to the reactor and vented to the atmosphere through a gas chromatograph (GC) or a soap flowmeter (SFM). Gas samples from the outlet of the reactor were continuously injected in a mass spectrometer (MS). The modulator and the mass spectrometer were interfaced to a minicomputer (DEC, PDP 11/34).

The gas flow rates were controlled at the entrance of the apparatus by mass flow controllers (Tylan, FIC 260), which provided accurate flow rates without temperature and pressure corrections. The range of the flow controllers was 0–100 cm^3/min. The back pressure in the apparatus was controlled by back pressure regulators at the exit of the modulator and of the reactor. Most of the piping was contained inside a convection oven with a continuous N_2 flush. The glass components in the apparatus were protected from overpressure by two relief valves in the helium and argon lines located inside the oven. These relief valves were set to 1 bar of pressure.

The saturator was a glass washbottle filled with methanol and was immersed in a constant-temperature bath. The washbottle was 50.8 mm in diameter and 101.6 mm long. The argon stream bubbled in the methanol through a distributor and left the washbottle at the top. For a 20 °C bath, the methanol concentration in argon was 11 mol %. The distributor was made of a fritted glass disk and was 12.7 mm in diameter and 25.4 mm in length.

The modulator periodically varied the composition of the feed to the reactor from helium to the argon/methanol mixture. The modulator consisted of a 0.159-mm chromatographic valve (VALCO), a helical drive air actuator (Valco Instruments, Model A-T-6-90°), two pilot valves (Humphrey, Model 125A-3-10), and a digital valve interface (Valco Instruments, Model DVI). The digital valve interface was an electronic controller that received the TTL signal from the computer and supplied air signals to the pilot valves. Upon receiving the air signal, the pilot valves allowed the entrance of high-pressure air (6.4 bar) into the helical drive moving the chromatographic valve 90°. The switching time for this system was about 100 ms.[27] The modulator was connected to the reactor through metal and glass capillaries. The two capillaries were connected by a 0.3175-mm swagelock fitting drilled inside to minimize dead volumes.

The reactor shown in Figure 4 consisted of a glass tube (6.4-mm i.d., 9.6-mm o.d., and 76.2 mm in length) surrounded by an aluminum jacket and inserted into a ceramic heater. The catalyst packing consisted of ground particles of 100–200 mesh size (74–149-μs U.S. Sieve size) and was supported in the glass tube by small portions of glass wool. The glass tube containing the packing was connected to the swagelock tee by a cajon metal–glass joint. The reactor was mounted vertically in the apparatus. From the modulator, the gas entered the top of the reactor through the glass capillary (0.7-mm i.d., 6.4-mm o.d., and 31.8 mm in length), reacted on the catalyst packing, and left the reactor at the bottom. The sampling tube and the reactor thermocouple were positioned right at the outlet of the catalyst packing and passed through the swagelock tee to the outside of the reactor. Samples were pumped into the mass spectrometer, and the temperature was continuously recorded.

The mass spectrometer (Balzers QMG 511) continuously analyzed the composition of the gas leaving the catalyst bed. The samples were admitted to the spectrometer through the Balzers minigas inlet system. The gas samples were pumped from the reactor through a 914.4-mm-long capillary tube (0.0472-mm diameter). The intermediate pressure in the inlet system valve body was 0.7 mbar. A small amount of gas leaked to the vacuum chamber through a small aperture (0.01 mm in diameter) in the valve body. The rest of the gas was pumped out of the inlet system valve via a throttle line by a rotary vane pump. The gas composition was analyzed by computer-controlled mass scanning of selected mass numbers. In this study, concentrations of water, methanol, argon, and dimethyl ether were measured at mass numbers 18, 31, 40, and 45, respectively. The computer system consisted of the PDP 11/34 system, a printer (DECwriter II), a graphics terminal (Tecktronix, Model 4014), and interfaces for the mass spectrometer and for input/output of TTL signals to the modulator. The operating system was the RT-11/SJ, and a set of FORTRAN IV programs controlled the experiments.

In general, the computer programs consisted of reading and setting the mass spectrometer controls. The settings of the mass values and fractions were supplied from a mass spectrometer calibration run. The desired experimental conditions such as the number of pulses and the number of points in each pulse were supplied to the programs at the beginning of the run. The data acquisition loop consisted of reading the mass spectrometer intensities, accumulating the intensity signals, reading the clock counting, and opening and closing the modulator's valve. At the

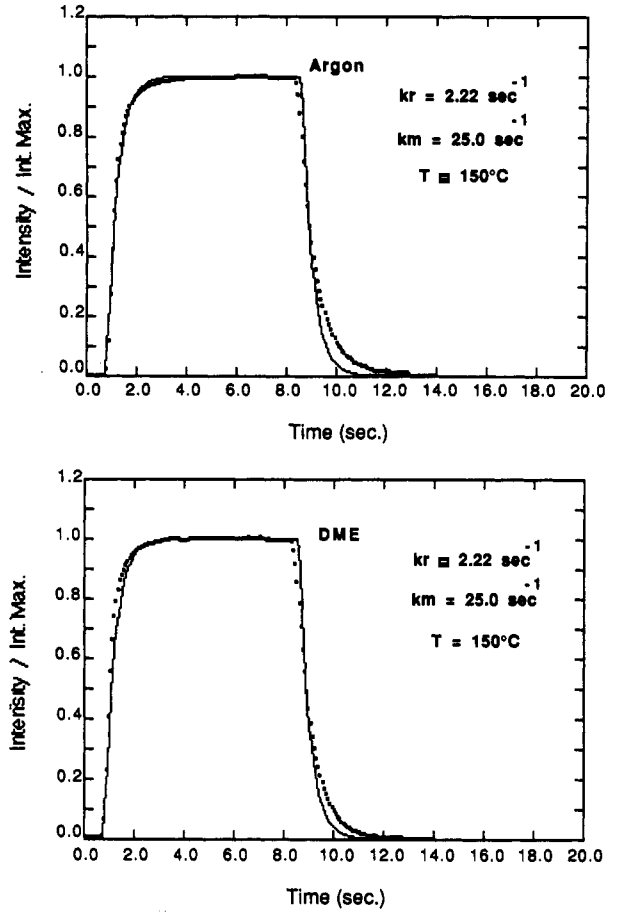

Figure 5. Argon and DME wave forms over inert packing: (—) model (eq 1); (···) experimental data.

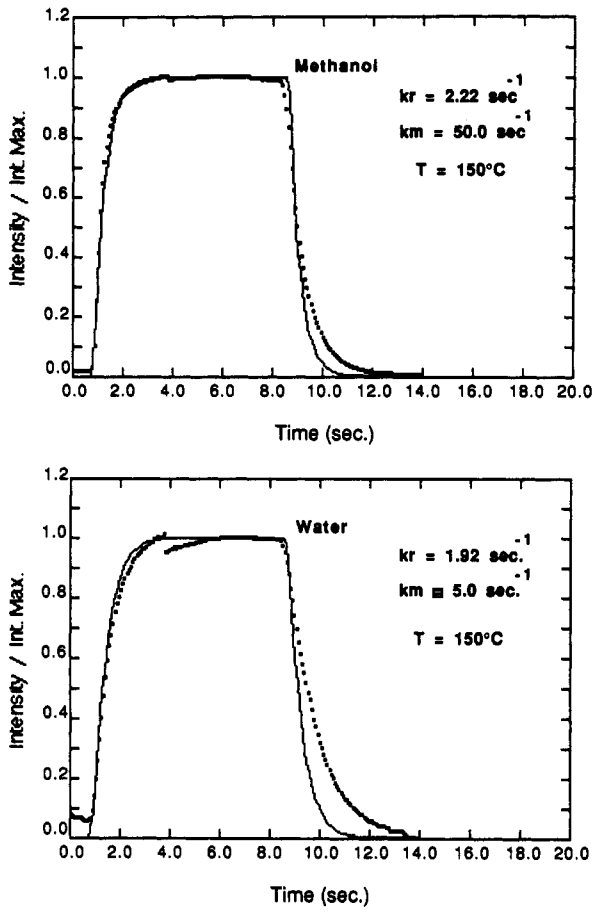

Figure 6. MeOH and water wave forms over inert packing: (—) model (eq 1); (···) experimental data.

end of the run, the accumulated signals were averaged and the clock counting was converted to the appropriate time units. The raw ion intensities and the averaged data were written to the hard disk on user's supplied file names. These files were water plotted on the Tecktronix terminal as the mass spectrometer intensities against the converted clock counting.

The calibration program that was used before every run determined the peak maximum for helium, argon, and methanol and optimized the mass spectrometer sensitivity. This measurement also gave the feed composition for argon and methanol. A steady-state run on the same catalyst sample preceded every periodic operation run.

A series of blank experiments were conducted to access the importance of the reactor mixing and spectrometer mass discrimination effects on the shape of the wave forms. These experiments consisted of measuring wave forms with the reactor filled with inert nonporous particles (silicon carbide). A mixture with composition of 53.5% argon, 32.2% dimethyl ether, 11.3% methanol, and 3.0% water was fed to the reactor, and the residence time distributions for each component were measured in the mass spectrometer.

The normalized mass spectrometer intensities as a function of time for each component are shown in Figures 5 and 6. These data were taken at a temperature of 150 °C, with an injection time of 7.2 s and a 50% duty cycle. Initially, there was a transport lag of about 0.81 s, from the opening of the valve until the breakthrough of the components in the analyzer. The rise time measured on the leading edge of the wave form was 0.82 s for DME, 0.93 for argon and methanol, and 1.6 s for water. When the valve was closed, the concentrations remained at their maximum levels for a time equal to the transport time and then decayed to zero. The pulse width at half-amplitude was 8.13 s for argon, 8.22 s for DME, 8.21 s for methanol, and 8.41 s for water.

These results are compared with the model of two well-mixed vessels connected in series. In the model, the time response of the concentration to a step change in the feed concentration is given by the following equation:[28]

$$C(t) = 1 - \frac{k_m e^{-k_r t} - k_r e^{-k_m t}}{k_m - k_r} \qquad (3)$$

where k_m and k_r are reciprocals of the residence time in the two vessels. One vessel was assigned to the reactor and the other to the mass spectrometer measuring chamber. Calculated pulses using eq 3 are shown in Figures 5 and 6 as solid lines. Values for k_m and k_r for best fit of eq 3 to the data were found by minimizing the sum of the squares of the deviation between the experimental and calculated curves. For argon and DME, the values of best fit for k_r and k_m were 2.22 and 25.0 s^{-1}, respectively. For methanol, k_r and k_m were 2.22 and 50.0 s^{-1} and for water, 1.92 and 5.0 s^{-1}.

These results show that the residence times in the reactor were about the same for all components (0.45 s for argon, DME, and methanol and 0.52 s for the water). The residence times in the mass spectrometer chamber were about 0.04 s for argon and DME, about 0.02 s for methanol, and about 0.2 s for water. The value of 0.45 s for the residence time in the reactor was close to the mean residence time of 0.50 s calculated from the ratio of the reactor volume (0.42 cm^3) with the volumetric flow rate (50 cm^3/min). In conclusion, the results from the blank experiments supported the assumption that reactor mixing and mass discrimination effects on the mass spectrometer were negligible in the experimental apparatus.

The catalyst used in this study was the commercial Harshaw 1602 γ-Al_2O_3 catalyst. The catalyst was heated to 450 °C under helium flow to eliminate the water from the solid and the surface. The effluent gas from the reactor was continuously sampled to the mass spectrometer to follow the water loss from the catalyst.

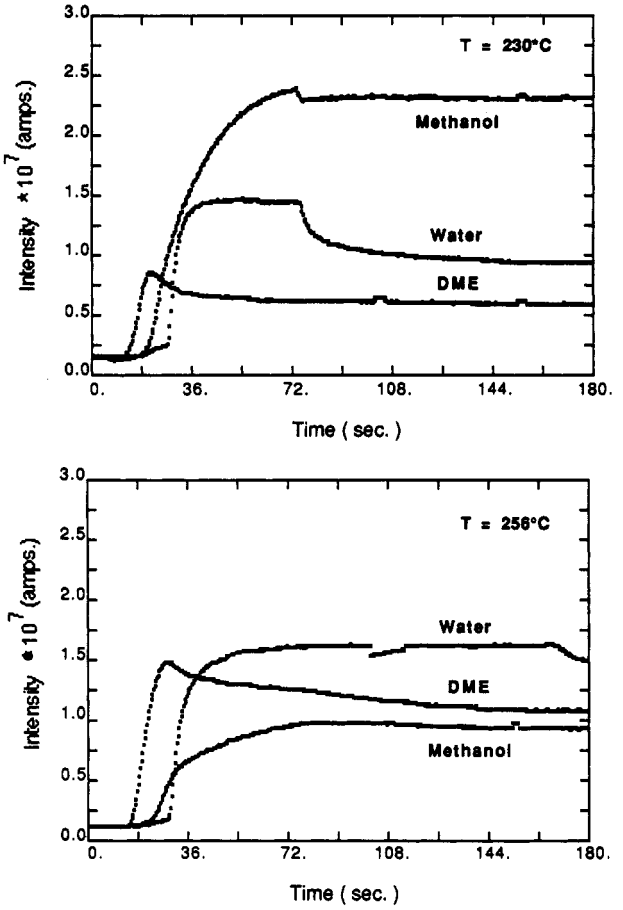

Figure 7. Reaction start-up: T = 230 and 256 °C.

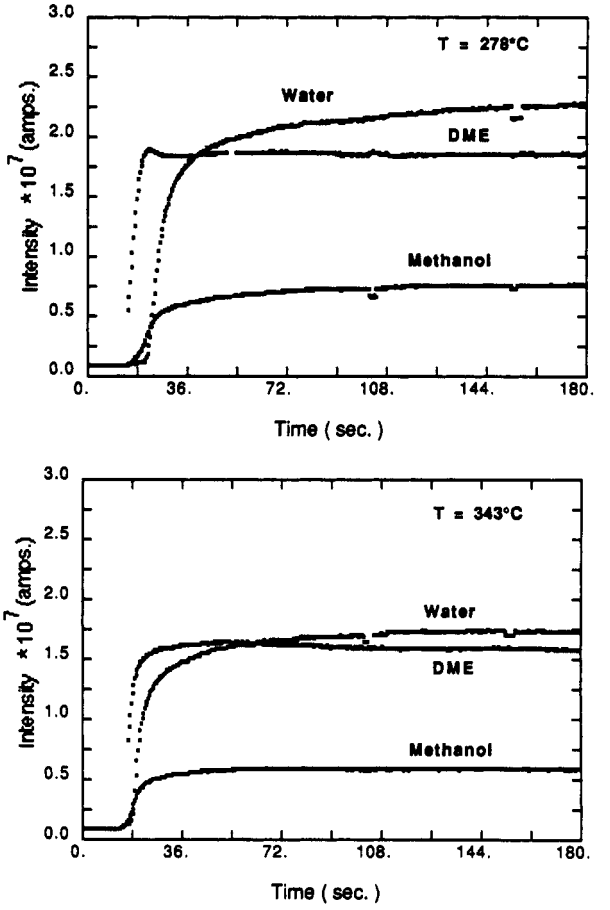

Figure 8. Reaction start-up: T = 278 and 343 °C.

The dehydration process continued until the water signal approached the background level of the mass spectrometer which typically required about 2 h. After the dehydration step, the reactor temperature was lowered to the desired temperature range of 230–345 °C for the experiments. The operating pressure was about 1 bar.

Results

The approach of the reaction to the steady state for the temperatures of 230, 256, 278, and 343 °C is shown in Figures 7 and 8. Each run was taken with a fresh load of catalyst (about 140 mg) following pretreatment at 450 °C. Curves for DME, methanol, and water are shown for each run. All components left the reactor after at least a 15-s delay time. Although there are some unexplained discontinuities in the curves, see, for example, methanol and water at 72 s for T = 230 °C and water at 90 s for T = 256 °C, the concentrations as a function of time are represented well. For all temperatures, the DME curve passed through a maximum at early times and then approached the steady value by 180 s. The methanol and water approached the steady value monotonically, but water curves continued to increase slightly even at 180 s for the higher temperatures.

At higher temperatures (Figure 8), the rise times to the steady state are larger than for the lower temperatures. The DME maximum is barely evident at 278 °C, and no breaks on the methanol curves are observed at either temperature. The breakthrough of the components from the reactor is in the order DME, methanol, and then water. The disparity in these breakthrough times decreases with temperature. By T = 343 °C, the methanol and water breakthrough times are nearly identical.

The results for periodic operation for the temperatures of 230, 256, 278, and 343 °C are shown in Figures 9–12. The injection time for these runs was 9.7 s (period 19.4 s), and the duty cycle was 50%. The wave forms are plotted as the mass spectrometer

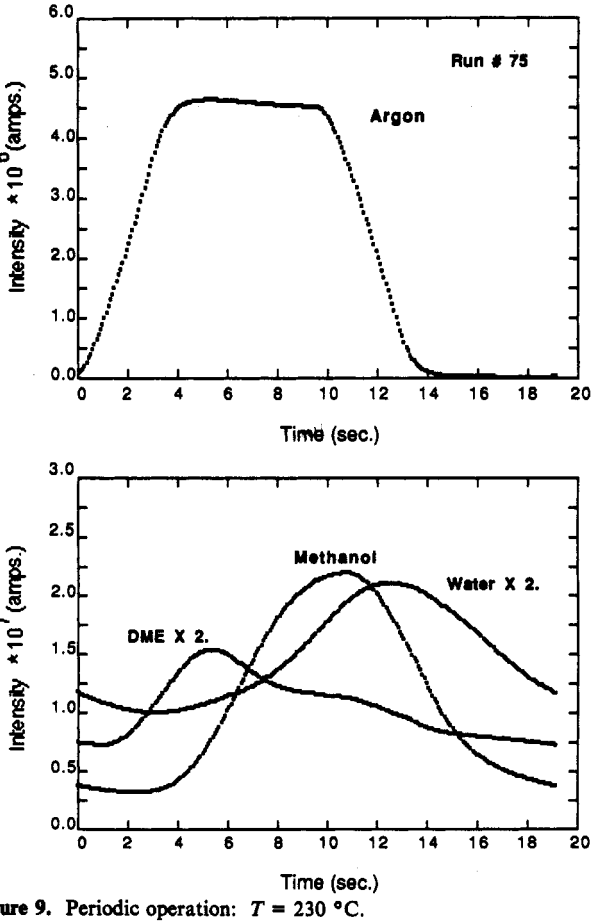

Figure 9. Periodic operation: T = 230 °C.

peak intensities against the time after the opening of the modulator valve. The upper graph shows the argon wave form and the

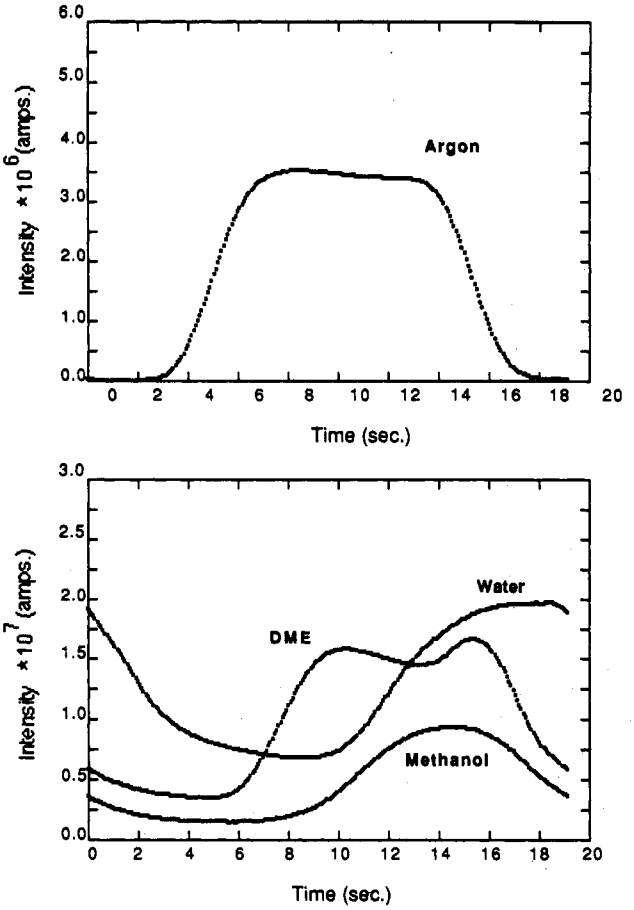

Figure 10. Periodic operation: T = 256 °C.

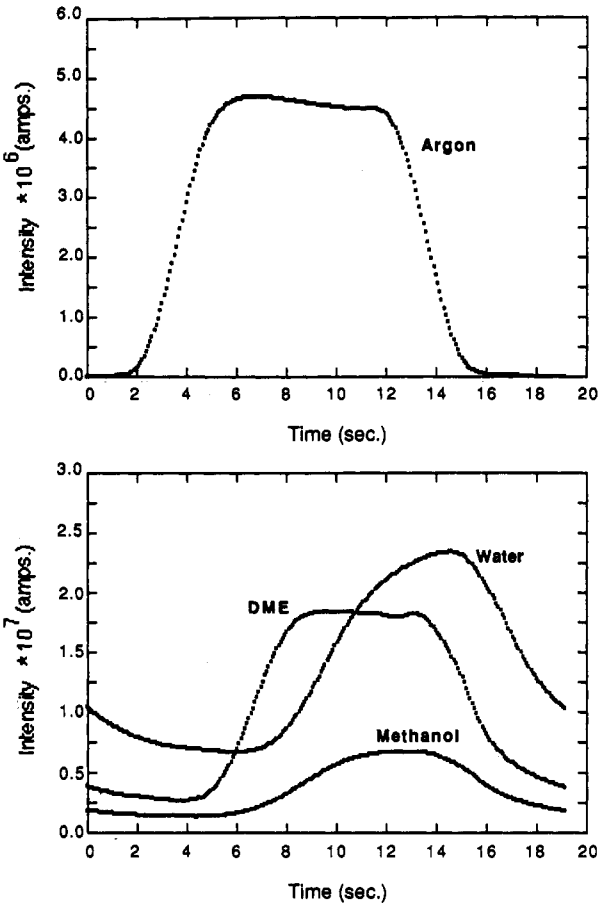

Figure 11. Periodic operation: T = 278 °C.

lower graph the DME, methanol, and water wave forms. The argon peak intensities are at least 10 times greater than the peak intensities of all the other components.

For temperatures lower than 280 °C, the DME wave form passes through two maxima: one in the first few seconds and a second at the beginning of the off cycle. The second maximum increases in amplitude as a function of temperature, but like the first maximum, it is quenched by 280 °C.

The methanol curve always rises monotonically to a maximum level during the first half of the cycle. The rise in the methanol wave form has a S shape, and the inflection point usually correlates with the first maximum in the DME wave form. The decay of methanol wave form during the last half of the cycle usually took about 2 s, for all temperatures.

The water curve rises monotonically in a S shape. It trails the DME curve by about 4–5 s. The water wave form is similar to the methanol curve, but it is broader and phase shifted. As a result, finite concentrations are still high during the last half of the cycle when DME and methanol concentrations are at minima.

The correlation of the inflection point in the methanol wave form with the first maximum in the DME wave form and the differences in shape between the DME and water wave forms suggested that DME and water were produced independently of each other from the catalyst. This feature could be used in the development of process schemes where the reaction and separation of the products can be achieved in the same unit operated under periodic conditions. The DME–water separation was larger with the reactor operated at a 33% duty cycle, as shown in Figure 13 for an injection time of 10 s and a period of 30 s.

On the average from all runs, DME, methanol, and water breakthrough times were delayed with respect to argon by about 2.6, 5.2, and 7.1 s, respectively. These results indicate that the catalyst held water more strongly than DME and that the water retained probably prevented further adsorption of methanol.

Discussions

These experimental results of the periodic operation of the methanol dehydration reaction presented remarkable differences between the DME and water wave forms. First, no direct correlation was seen between the DME and the water wave forms, and the water wave form on average trailed behind the DME wave form by about 4 s. This independence of the water and DME wave forms suggested the presence of two independent reaction steps for the production of DME and water in the mechanism. Furthermore, the change in the shape of the DME wave form with temperature suggested that the DME production would itself include two reaction pathways.

These reaction steps can be formulated into the following kinetic model for the dehydration of methanol on the alumina catalyst:

(1) $CH_3OH(g) \leftrightarrow CH_3OH(a), \quad k_1, k_6$

(2) $O + CH_3OH(a) \rightarrow CH_3O(a) + OH, \quad k_2$

(3) $CH_3OH(a) + CH_3O(a) \rightarrow CH_3OCH_3(g) + OH, \quad k_3$

(4) $CH_3O(a) + CH_3O(a) \rightarrow CH_3OCH_3(g) + O, \quad k_4$

(5) $2OH \rightarrow H_2O(g) + O, \quad k_5$

The first step is the reversible adsorption of methanol on the surface. The surface was assumed to be covered with surface oxide, indicated as O. The methanol molecule adsorbs on a surface site and covers up one or more surface oxides, generating molecular adsorbed methanol species. In step 2, molecular adsorbed methanol reacts with a surface oxide and dissociates, forming a methoxy group and an hydroxyl group. A surface reaction between two different species could explain the maximum in the

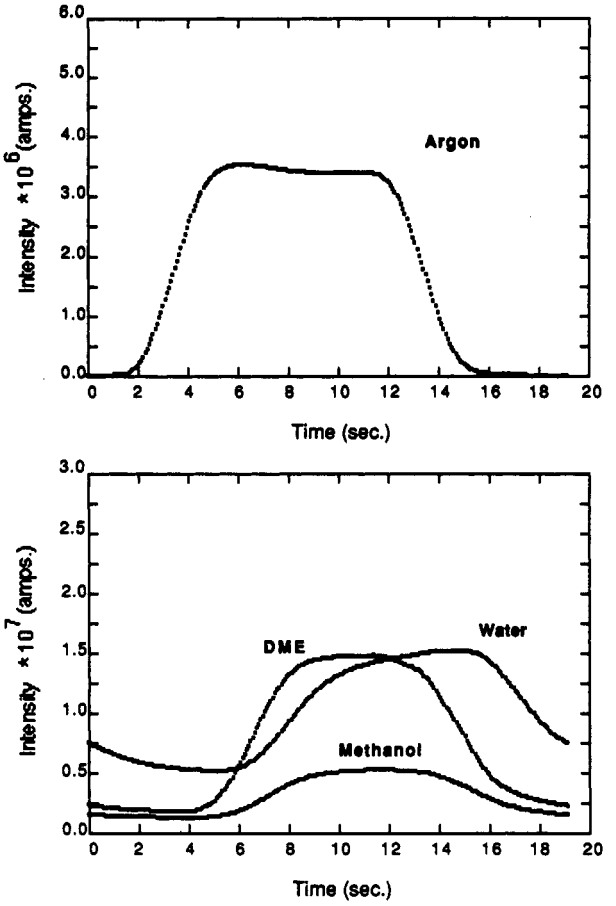

Figure 12. Periodic operation: T = 343 °C.

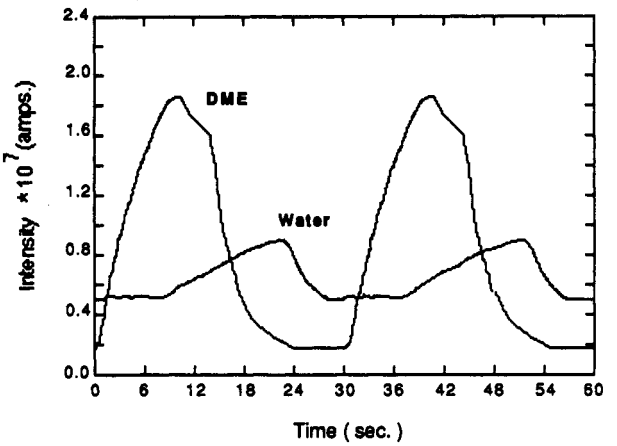

Figure 13. Periodic operation: T = 343 °C; 25% duty cycle; DME and water separation.

DME wave form. One possibility is the reaction of molecularly adsorbed methanol, coordinated to the surface, and the methoxy group (step 3). A second possibility is the reaction between two surface methoxy species (step 4). This reaction could lead to a maximum in DME formation only if there were a maximum in the surface methoxy concentration. The recombination of OH groups (step 5) produced water, which in this reaction sequence is assumed to desorb immediately into the gas phase, but it is also possible that water is retained on the surface on the molecular state before desorption.

The shape of the experimental wave forms could be reproduced by solving the equations for this kinetic scheme taking place in a well-mixed flow reactor. The system of equations for the dimensionless concentrations describing the dynamic response of the system is the following:

$$\mathrm{dMe}/\mathrm{d}t = -k_1\mathrm{MeO} - k_n\mathrm{Me} + k_r f + k_6\mathrm{Ma}$$

$$\mathrm{dMa}/\mathrm{d}t = k_1\mathrm{MeO} - k_2\mathrm{MaO} - k_3\mathrm{MaMt} - k_6\mathrm{Ma}$$

$$\mathrm{dMt}/\mathrm{d}t = k_2\mathrm{MaO} - k_3\mathrm{MaMt} - k_4\mathrm{Mt}^2$$

$$\mathrm{dOH}/\mathrm{d}t = k_2\mathrm{MaO} + k_3\mathrm{MaMt} - 2k_5\mathrm{OH}^2$$

$$\mathrm{dD}/\mathrm{d}t = k_3\mathrm{MaMt} + k_4\mathrm{Mt}^2 - k_r\mathrm{D}$$

$$\mathrm{dW}/\mathrm{d}t = k_5\mathrm{OH}^2 - k_r\mathrm{W}$$

$$1 = \mathrm{O} + \mathrm{Ma} + \mathrm{Mt} + \mathrm{OH} \qquad (4)$$

where the following notation for the concentration terms was adopted: f, concentration of methanol in the feed to the reactor; Me, methanol in the gas phase inside the reactor; Ma, molecularly adsorbed methanol; Mt, surface methoxy groups; O, surface oxide; OH, surface hydroxyl groups; D, dimethyl ether in the gas phase inside the reactor; and W, water in the gas phase inside the reactor.

It was assumed that the methanol adsorption is proportional to the gas-phase concentration, Me, and to the surface oxide concentration, O. The last relationship in eq 4 implied that the surface was always covered with a monolayer of species. Before the adsorption of any reactive species, the clean surface consisted entirely of oxide coverage.

The system of eq 4 was integrated numerically using the fourth-order Runge–Kutta method and using a square-wave input for the methanol concentration in the feed to the reactor. Starting initially with finite methanol concentration in the reactor and the concentrations of surface species equal to zero, the simulations were run sequentially from the methanol mass balance to the water mass balance for 256 data points. The simulations continued until the last point in the wave form was equal to the first point. It usually took five pulses to reach the condition of a steady wave form. The step size in the Runge–Kutta method was calculated as 0.078 125, corresponding to a period of 20 s over 256 points.

For a square-wave maximum of 0.1, the wave forms for gas-phase species (methanol, DME, and water) and for surface species (methanol adsorbed, methoxy, hydroxyl, and oxide) were calculated. Each wave form was scaled with its own maximum value. Figures 14 and 15 show the normalized concentrations for a simulation run using the following values of dimensionless rate parameters: k_r = 2.2; k_1 = 30.0; k_2 = 0.375; k_3 = 1.5; k_4 = 0.01; k_5 = 0.6; and k_6 = 1.0.

The methanol wave form showed a monotonic increase for the first half-cycle with almost a constant slope between 0 and 5 s, followed by a decrease in slope at 5 s until the end of the half-period (Figure 14). The oxide concentration decreased monotonically as the surface became covered with other surface species, such as methanol adsorbed, methoxy, and hydroxyls. The DME wave form shown in Figure 14 had a maximum at about 4 s and decreased to a constant level during the on cycle. The methanol adsorbed wave form increased monotonically in a similar way as the methanol in the gas phase, representing the propagation of the forcing from the gas phase to the surface.

The methoxy wave form increased first, went through a maximum at about 2 s, decreased until the end of the on cycle, and increased monotonically during the off cycle. The maximum in the methoxy concentration coincided with the crossing of the methanol and oxide wave forms at 2 s. The crossing of the methanol adsorbed and methoxy wave forms at 4 s, gave the maximum in the DME wave forms. No maxima were observed in these simulation runs at the beginning of the off cycle.

The water and hydroxyls concentrations are shown in Figure 15. They both had a monotonic increase during the first half of the period. The water lagged the hydroxyls by about 0.5 s as seen

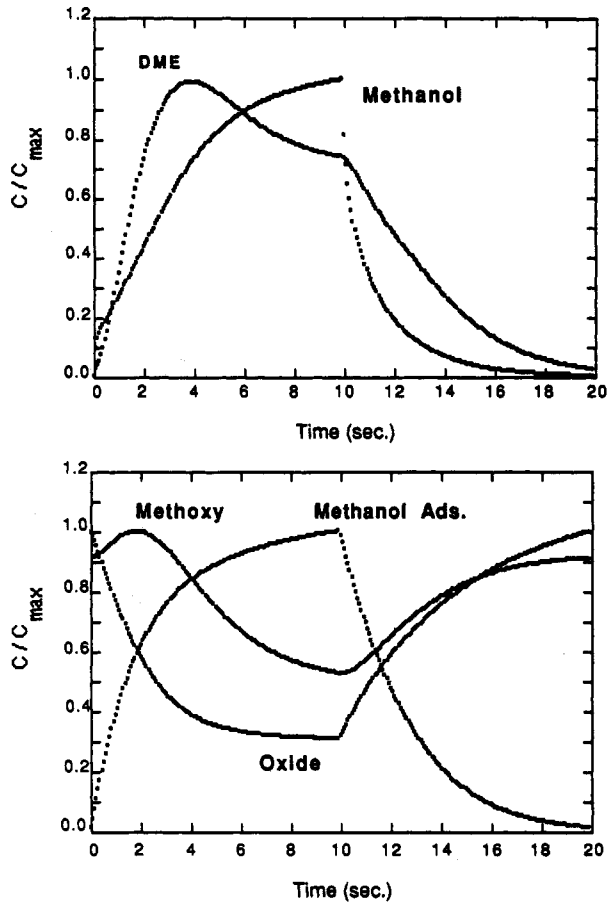

Figure 14. Methanol, DME, methanol adsorbed, methoxy, and oxide simulations.

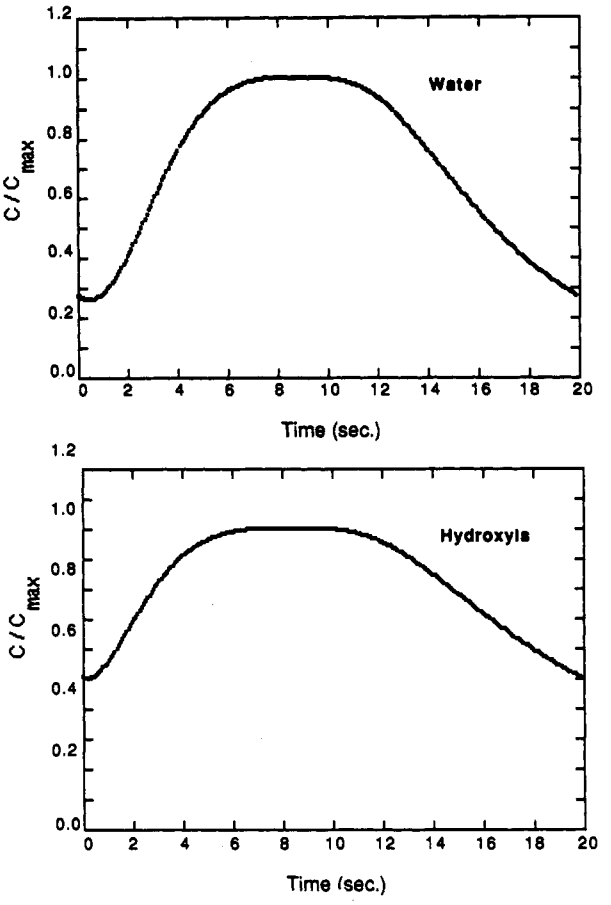

Figure 15. Water and hydroxyls simulations.

from the time the wave forms reached the maximum. Both wave forms were uncorrelated with the methanol and the methoxy wave forms.

The results of a second simulation run with $k_3 = 0.1$ and $k_4 = 6.0$ and all other rate constants the same are shown in Figure 16. The methanol, methanol adsorbed, and oxide results were approximately the same as before, but the methoxy and the DME wave forms showed a double maxima. The first maximum in the methoxy concentration at about 4 s corresponded to the usual maximum observed in kinetic schemes containing an intermediate and a subsequent reaction to form products. The second maximum in the methoxy concentration occurred about 2 s after the beginning of the off cycle (12 s), and it was due to the crossing of the methanol adsorbed and oxide wave forms. The double maxima in the DME wave form was a mapping of the double maxima present in the methoxy concentration. Thus, the methoxy–methoxy reaction dominated the double-maxima structure in the DME wave form. The water wave form had a similar monotonic increase as calculated in the first simulation.

The results for a third simulation run with $k_r = 4.0$, $k_3 = 0.09$, and $k_4 = 0.2$ and all other rate constants the same are shown in Figure 17. The methanol, methanol adsorbed, and oxide results had a more squared shape than previous simulation runs. The methoxy wave form had a maximum at about 3 s after the beginning of the off cycle. This maximum occurred without any simultaneous crossing of the methanol adsorbed and oxygen curves. The DME wave form had only a broad maximum approaching a flat top wave form. The water and hydroxyl results showed only a monotonic increase to a maximum that occurred at the end of the on cycle.

From the periodic operation data and the nonlinear simulation results, the appearance of a maximum in the DME wave form indicated that at least one branch in the reaction sequence was nonlinear. Two types of surface reactions could be involved in the production of DME: the reaction between methanol and methoxy and the reaction between two adsorbed methoxy groups. Also, if the surface methoxy species were formed by the removal of H from adsorbed methanol, this step could lead to a maximum in the methoxy concentration which could then cause a maximum in the methoxy–methoxy reaction channel.

The temperature effect on the shape of the DME wave forms is shown in Figure 18 for the temperatures of 230, 248, 256, and 280 °C. The curves were normalized and adjusted to the same origin for the comparison. The 230 °C curve had a maximum at about 6 s and a constant level part until about 10 s. The 248 °C curve had also a maximum around 6 s and a higher constant level part than the 230 °C curve. The 256 °C curve had two maxima: one around 6 s, coinciding with the maxima of the 230 and 248 °C curves, and a second maxima at 12 s after the constant level part. Finally, the 280 °C curve showed simply a monotonic increase to a constant level.

As in the case for all reaction intermediates, the methoxy concentration will pass through a maximum. If the methanol concentration was still increasing from adsorption from the gas phase after the methoxy maximum, then the methoxy–methanol reaction could be expected to pass through a maximum when the concentrations of methoxy and adsorbed methanol cross with opposite slopes. At intermediate temperatures, the second maximum observed at turn-off corresponds to the crossing of the methanol adsorbed and methoxy curves. At higher temperatures, either an increase in the methanol desorption rate or an increase in the rate of formation of methoxy could be responsible for suppressing the maximum.

Note that the observed first maximum in the DME wave form was not due to the breakthrough of DME from the bed by replacement of more strongly adsorbed species, such as methanol or water. If these effects were present, the methanol curve would also present a maximum at the beginning of the wave form, but this was not observed.

The water wave forms showed always a monotonic increase at all temperatures. The water formation could be attributed to the

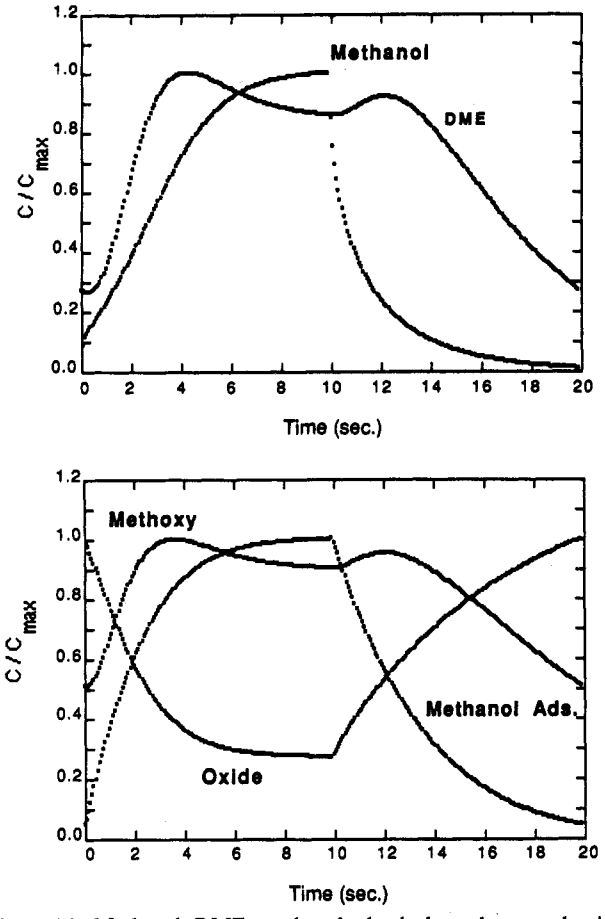

Figure 16. Methanol, DME, methanol adsorbed, methoxy, and oxide simulations.

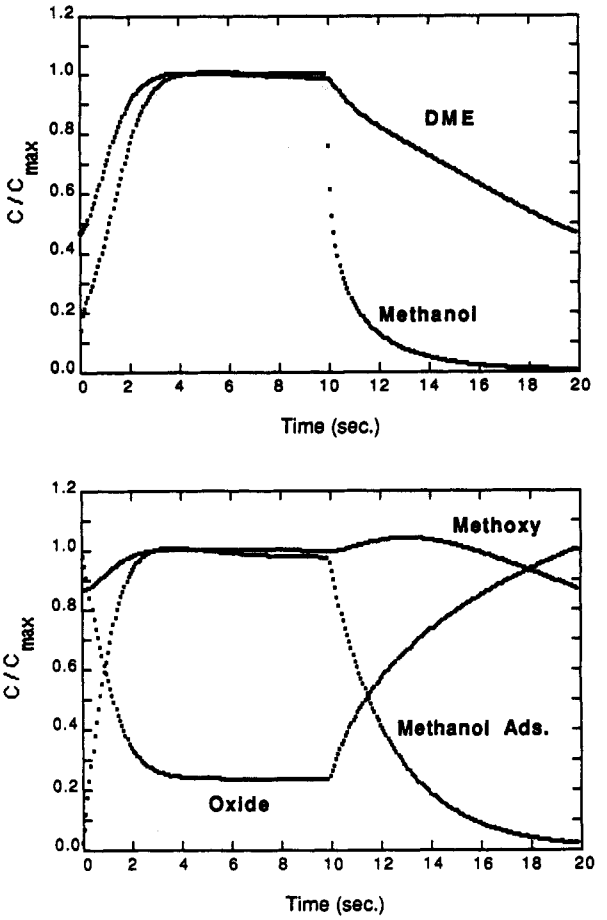

Figure 17. Methanol, DME, methanol adsorbed, methoxy, and oxide simulations.

recombination of surface OH groups, as in a normal dehydration process. The recombination and subsequent desorption of water were relatively slower than the production of DME so that a time lag of as much as 4 s was established in all runs. Even unreacted methanol left the reactor before the water, which was consistent with the inhibiting effect of water in the methanol adsorption.

The shapes of the wave forms reported here were in general agreement with a recent study published by Moravek[29] on the dehydration of alcohols on alumina and with a study of the ethanol dehydration of an ion-exchange resin by Dennis and Kabel.[30] In Moravek's study, the ethanol dehydration to alkenes was described by the Ipatiev–Hinshelwood kinetic model which included the inhibition of the reaction rate by water. In Dennis and Kabel's study, the ether response went through a maximum first and then decreased to reach the new steady-state value following a step decrease in the ethanol flow rate. The water response continuously increased to the new steady-state value.

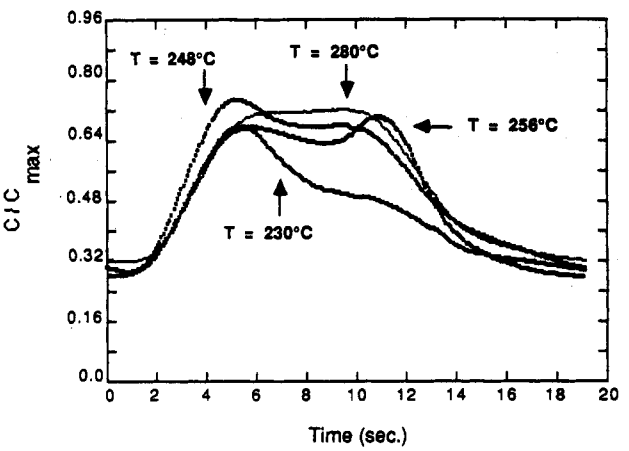

Figure 18. Temperature effect on DME wave form.

Conclusions

The periodic operation of the methanol dehydration on γ-Al_2O_3 catalyst indicated that the products are formed from the surface reaction of species formed from the methanol adsorption. The dissociative adsorption of methanol forms methoxy and hydroxyl groups which undergo two independent reaction steps producing dimethyl ether and water, respectively. The dimethyl ether was weakly adsorbed onto the catalyst surface and left the reactor at least 10 reactor residence times before the water, which was strongly adsorbed.

In addition to the methoxy–methoxy reaction pathway, the periodic operation data indicated that dimethyl ether can also be formed from the reaction of molecularly adsorbed methanol and methoxy species. This channel was evident at temperatures below 280 °C. Above 280 °C, the predominant channel for the dimethyl ether formation was the reaction of two methoxy species. The recombination of hydroxyls and subsequent desorption of water from the γ-Al_2O_3 catalyst was slower than the formation of dimethyl ether from both pathways.

The difference in the rates of formation of dimethyl ether and water could be regarded as an advantage for periodic operation over steady-state operation of chemical reactors used for methanol dehydration reaction. This advantage would allow obtaining reaction and product separation in a single vessel operated under period conditions as opposed to conventional distillation units downstream from the reactor.

Acknowledgment. We are thankful to Prof. Arthur Sleight of Oregon State University for his support and interest in this research, to Dr. Christian Machiels (posthumously), and to Mr. John Borowski. This work was financially supported by the E.

I. du Pont de Nemours & Co. which included the permission for conducting the experiments at Experimental Station, Wilmington, DE.

References and Notes

(1) Douglas, J. M. *Ind. Eng. Chem. Process Des. Dev.* **1967**, *6*, 43.
(2) Horn, F. J. M.; Lin, R. C. *Ind. Eng. Chem. Process Des. Dev.* **1967**, *6*, 21.
(3) Bailey, J. E.; Horn, F. J. M. *AIChE J.* **1967**, *17*, 550.
(4) Bailey, J. E. *Chem. Eng. Commun.* **1974**, *1*, 11.
(5) Renken, A. *Chem. Eng. Sci.* **1972**, *27*, 1925.
(6) Renken, A. *Chem.-Ing.-Tech.* **1982**, *54*, 571.
(7) Silveston, P. L. *Sādhanā* **1987**, *10*, 217.
(8) Unni, M. P.; Hudgins, R. R.; Silveston, P. L. *Can. J. Chem. Eng.* **1973**, *51*, 623.
(9) Renken, A.; Müller, M.; Wandrey, C. *Proc. 4th Int. Symp. Chem. Reaction Eng.* **1976**.
(10) Bilimoria, M.; Bailey, J. *ACS Symp. Ser.* **1978**, *65*, 526.
(11) Dettmer, M.; Renken, A. *Ger. Chem. Eng.* **1983**, *6*, 356.
(12) Siddall, J. H.; Miller, M. L.; Delgass, W. N. *Chem. Eng. Commun.* **1989**, *83*, 261.
(13) Austin, G. T. *Sherve's Chemical Process Industries*, 5th ed.; McGraw-Hill: New York, 1984.
(14) Cocke, D. L.; Johnson, E. D.; Merrill, R. P. *Catal. Rev.-Sci. Eng.* **1984**, *26* (2), 163.
(15) Satterfield, C. N. *Heterogeneous Catalysis in Practice*; McGraw-Hill: New York, 1980.
(16) Lippens, B. C.; Steggerda, P. In *Physical Chemical Aspects of Adsorbents and Catalysis*; Linsen, B. G., Ed.; Academic Press: New York, 1970.
(17) Peri, J. B. *J. Phys. Chem.* **1965**, *69*, 220.
(18) Knözinger, H.; Ratnasmy, P. *Catal. Rev.-Sci. Eng.* **1978**, *17* (1), 31.
(19) Dabrowski, J.; Butt, J.; Bliss, H. *J. Catal.* **1970**, *18*, 297.
(20) Stair, P. C. *J. Am. Chem. Soc.* **1982**, *104*, 4044.
(21) Busca, G.; Rossi, P. F.; Lorenzelli, V.; Benaissa, M.; Travert, J.; Lavalley, J. *J. Phys. Chem.* **1983**, *89* (25), 5433.
(22) Staley, R. Private communication, 1986.
(23) Knözinger, H.; Scheglila, A.; Watson, A. M. *J. Phys. Chem.* **1968**, *79* (8), 2770.
(24) Notari, B. *Chim. Ind.* **1969**, *51*, 1200.
(25) Figueras, F.; Nohl, A.; De Mourgues, L.; Tramboze, Y. *Trans. Faraday Soc.* **1971**, *67*, 1155.
(26) Matsushima, T.; White, J. M. *J. Catal.* **1976**, *44*, 183.
(27) Harvey, M. C.; Stearns, S. D. *Anal. Chem.* **1984**, *56*, 837.
(28) Coughanowr, D. R.; Koppel, L. B. *Process Systems Analysis and Control*; McGraw-Hill: New York, 1965.
(29) Moravek, V. *J. Catal.* **1992**, *133*, 170.
(30) Denis, G. H.; Kabel, R. L. *AIChE J.* **1970**, *34*, 972.